Toxicology and Applied Pharmacology 252 (2011) 97–111

Contents lists available at ScienceDirect

Toxicology and Applied Pharmacology

journal homepage: www.elsevier.com/locate/ytaap

The enhanced value of combining conventional and "omics" analyses in early assessment of drug-induced hepatobiliary injury

Heidrun Ellinger-Ziegelbauer [a,*], Melanie Adler [b], Alexander Amberg [c], Arnd Brandenburg [d], John J. Callanan [e], Susan Connor [f], Michael Fountoulakis [g], Hans Gmuender [d], Albrecht Gruhler [h], Philip Hewitt [i], Mark Hodson [f], Katja A. Matheis [j], Diane McCarthy [k], Marian Raschke [l], Björn Riefke [l], Christina S. Schmitt [i], Max Sieber [b], Alexandra Sposny [i], Laura Suter [g], Brian Sweatman [f], Angela Mally [b]

[a] *Bayer Schering Pharma AG, Wuppertal, Germany*
[b] *University of Wuerzburg, Wuerzburg, Germany*
[c] *Sanofi aventis R&D, Disposition, Safety & Animal Research, Frankfurt, Germany*
[d] *Genedata AG, Basel, Switzerland*
[e] *UCD School of Biomolecular and Biomedical Science & School of Agriculture, Food Science & Veterinary Medicine, UCD Conway Institute, University College Dublin, Dublin, Ireland*
[f] *MetaPro, UK*
[g] *Hoffmann-La Roche AG, Basel, Switzerland*
[h] *Novo Nordisk A/S, Maaloev, Denmark*
[i] *Merck KGaA; Darmstadt, Germany*
[j] *Boehringer Ingelheim Pharma GmbH & Co. KG, Biberach, Germany*
[k] *Bio-Rad, Laboratories, Hercules, CA, USA*
[l] *Bayer Schering Pharma AG, Berlin, Germany*

ARTICLE INFO

Article history:
Received 10 June 2010
Revised 17 September 2010
Accepted 23 September 2010
Available online 1 October 2010

Keywords:
Preclinical safety assessment
Liver
Drug-induced hepatotoxicity
Toxicogenomics
Metabonomics

ABSTRACT

The InnoMed PredTox consortium was formed to evaluate whether conventional preclinical safety assessment can be significantly enhanced by incorporation of molecular profiling ("omics") technologies. In short-term toxicological studies in rats, transcriptomics, proteomics and metabolomics data were collected and analyzed in relation to routine clinical chemistry and histopathology. Four of the sixteen hepato- and/or nephrotoxicants given to rats for 1, 3, or 14 days at two dose levels induced similar histopathological effects. These were characterized by bile duct necrosis and hyperplasia and/or increased bilirubin and cholestasis, in addition to hepatocyte necrosis and regeneration, hepatocyte hypertrophy, and hepatic inflammation. Combined analysis of liver transcriptomics data from these studies revealed common gene expression changes which allowed the development of a potential sequence of events on a mechanistic level in accordance with classical endpoint observations. This included genes implicated in early stress responses, regenerative processes, inflammation with inflammatory cell immigration, fibrotic processes, and cholestasis encompassing deregulation of certain membrane transporters. Furthermore, a preliminary classification analysis using transcriptomics data suggested that prediction of cholestasis may be possible based on gene expression changes seen at earlier time-points. Targeted bile acid analysis, based on LC-MS metabonomics data demonstrating increased levels of conjugated or unconjugated bile acids in response to individual compounds, did not provide earlier detection of toxicity as compared to conventional parameters, but may allow distinction of different types of hepatobiliary toxicity. Overall, liver transcriptomics data delivered mechanistic and molecular details in addition to the classical endpoint observations which were further enhanced by targeted bile acid analysis using LC/MS metabonomics.

Introduction

Within recent years, several large-scale collaborative projects involving academic and industrial institutions as well as regulatory agencies have been initiated with the aim of delivering tools for improved preclinical safety assessment and prediction of toxicity. While the Predictive Safety Testing Consortium (http://www.c-path.org/pstc.cfm), a public–private partnership led by the non-profit Critical Path Institute (C-Path), focuses on qualifying pre-clinical

Abbreviations: Tx, Transcriptomics; Mx, Metabolomics; Px, Proteomics; LC/MS, Liquid chromatography followed by mass spectrometry; PP, peroxisome proliferation; XME, Xenobiotic metabolism; SVM, Support vector machine; HD, high dose; LD, low dose; LOQ, limit of quantification; CA, cholate; GCA, glycocholate; TCA, taurocholate; TβMCA, tauro-β-muricholate; ΔTβMCA, unsaturated tauro-β-muricholate; ALT, alanine aminotransferase; AST, asparate aminotransferase; ALP, alkaline phosphatase.

* Corresponding author. Bayer Schering Pharma AG, BSP-GDD-GED-TOX, Elb 514, Aprather Weg 18a, 42096 Wuppertal, Germany. Fax: +49 202 36 4137.
E-mail address: heidrun.ellinger-ziegelbauer@bayerhealthcare.com (H. Ellinger-Ziegelbauer).

0041-008X/$ – see front matter © 2010 Elsevier Inc. All rights reserved.
doi:10.1016/j.taap.2010.09.022

safety biomarkers of key problem toxicities, i.e. carcinogenicity, and kidney, liver, muscle and vascular injury, the Innomed-PredTox consortium (http://www.innomed-predtox.com) set out to assess the value of combining results from "omics" technologies together with results from conventional toxicology methods for more informed decision making in preclinical safety evaluation. "Omics" responses to 14 drug candidates, which previously failed during non-clinical development in part due to hepatotoxic and/or nephrotoxic effects, were extensively characterized and integrated with conventional endpoints to obtain better understanding of key mechanisms of toxicity and identify more sensitive safety biomarkers. This comprised systemic toxicity studies in rats treated with hepatotoxic or nephrotoxic compounds at two dose levels for 1, 3, or 14 days by oral gavage, with the high dose having previously been associated with organ toxicity after 14 days of exposure. Organ samples and body fluids were then analyzed both for conventional endpoints and by using "omics" technologies, including transcriptomics, proteomics and metabolomics.

Different principles may be used to group item expression profiles and select significantly deregulated items, with items representing either genes, metabolites or proteins in the case of transcriptomics (Tx), metabolomics (Mx) or proteomics (Px), respectively. An often used principle in toxicogenomics is grouping of item profiles according to classical toxicological endpoints (Mattes et al., 2004; Ganter et al., 2006), which may allow investigations of the molecular mechanisms associated with different phenotypes of toxicity, and the extraction of diagnostic or predictive item signatures after having conducted studies with a reasonable number of compounds.

To investigate molecular functions and pathways leading to or associated with a particular phenotype, studies conducted within the frame of the Innomed-PredTox project were grouped according to common liver or kidney pathologies (Suter et al., 2011). Four of the compounds, FP004BA, FP005ME, FP007SE and FP014SC, abbreviated in the following as 4BA, 5ME, 7SE, and 14SC, induced similar liver phenotypes involving both the liver parenchyma and the bile duct compartment (4BA, 5ME, 7SE) or at least bile homeostasis (14SC). In the present study, deregulated genes in the target organ liver were determined in relation to histopathological scores associated with samples showing hepatobiliary injury. These genes were then mapped to pathways or functions in the context of hepatotoxicity.

In addition to providing mechanistic insight, Tx profiles may be used to classify compounds with respect to the pathological phenotype they induce upon treatment (Ganter et al., 2006; Blomme et al., 2009). It can be expected that compounds eliciting similar pathologies affect the same or related mechanisms and are therefore likely to deregulate similar sets of genes in a comparable manner. These gene signatures may then be employed in a diagnostic or predictive manner. For example, expression profiles generated from rat liver after short term treatment would be used to predict the potential for a specific toxicity earlier than a clearly detectable histopathological lesion and aid the interpretation of classical parameter measurements. Since a major objective of Innomed-PredTox was more informed decision making earlier in preclinical safety evaluation, we evaluated the potential of Tx data obtained from studies showing hepatobiliary toxicity for early prediction of cholestasis. Similarly, to test the value of individual bile acids as sensitive markers of hepatobiliary injury and to shed further light on potential mechanisms associated with the cholestatic phenotypes seen in this study group, metabonomics LC/MS data was used to determine the effect of individual compounds on a range of conjugated and unconjugated bile acids in urine and serum.

Methods

In addition to the methods described here, further details on the methods and technologies used are given in the accompanying overview paper by Suter et al. (2011).

Animal treatment. All animal studies were conducted in accordance to European or national animal welfare regulations using a harmonized study protocol as previously described (Mulrane et al., 2008). Briefly, male Wistar rats (8–10 weeks old, weighing 170–200 g) were distributed into three dose groups ($n=5$ per group and time-point) and dosed with (+)-(1*R*)-1-[4-(4-fluorophenyl)-2,6-diisopropyl-5-propyl-pyridin-3-yl]ethanol (4BA) at 0, 20 and 100 mg/kg/day, (1-(2-trifluoromethoxyphenyl)-2-nitroethanone (5ME) at 0, 15 and 350 mg/kg/day, 3-pyrrolidineacetic acid, 5-[[[4′-[imino[(methoxycarbonyl) amino]methyl] [1,1′-biphenyl]-4-yl]oxy]methyl]-2-oxo-,methyl ester, (3S-*trans*) (7SE) at 0, 100 and 1000 mg/kg/day or tetraethyl[(3-hydroxy-2-pyridyl)amino]methanediphosphonate (14SC) at 0, 280 and 1120 mg/kg/day by oral gavage for 1, 3 or 14 days, followed by necropsy after an overnight fasting period. After 1, 3 and 12 days of dosing, 16 h urine samples were collected from those animals treated for a total of 14 days, aliquoted and stored at −80 °C until use. At necropsy, blood and serum was collected for clinical chemistry, hematology, metabonomics and blood transcriptomics as indicated below. Organs (liver, kidney) were removed, aliquoted, fixed in formalin or flash frozen in liquid nitrogen and stored at −80 °C. Sections (3–4 mm) were fixed in 10% phosphate buffered formalin and subsequently embedded in paraffin blocks, sectioned, stained with hematoxylin and eosin and examined by light microscopy by the respective study pathologist.

Immunohistochemistry. Immunohistochemical staining of proliferating cell nuclear antigen (PCNA), neutrophile gelatinase associated lipocalin (NGAL/lipocalin-2) and tissue inhibitor of metalloproteinases 1 (TIMP1) was performed on tissue microarrays as previously described (Adler et al., 2010; Hoffmann et al., 2010). Antibodies used were a monoclonal anti-mouse PCNA (sc-56, Santa Cruz, 1:400), a goat anti-rat lipocalin-2/NGAL (R&D Systems GmbH, Wiesbaden-Nordenstadt, Germany), and a rabbit anti-human TIMP1 (Millipore, Schwalbach, Germany, 1:400).

Transcriptomics. Approximately 100 mg of frozen tissue was homogenized for total RNA extraction using RNeasy columns (Qiagen). Purified total RNA was submitted to DNase digestion using RNase-Free DNase (Qiagen) before 5 µg purified total RNA were used for cDNA synthesis, in vitro transcription, and fragmentation using the GeneChip Expression 3′ Amplification One-Cycle Target Labeling kit and Control Reagents (Affymetrix). Fragmented in vitro transcripts (cRNAs) were hybridized onto RAE 230_2.0 microarrays (Affymetrix), scanned and used for further analysis. Microarray quality was evaluated using the Refiner software (Genedata). Statistical gene expression analysis was performed using Expressionist (Genedata).

Selection of deregulated genes by statistical methods. Expression values for all probe sets were obtained by applying the Robust Multi-array Average (RMA) condensing method to batches of arrays corresponding to the same compound. In order to normalize the data and to make them comparable across all studies, all condensed probe set expression values of the treated animal samples of a given study were divided by the median of the respective time-matched vehicle group. Subsequently, the data from individual vehicle samples were normalized in this way.

Positive and negative groups of samples were defined based on the histopathology scores as follows. The histopathology terms "hepatocyte cell death", "bile duct epithelial cell mitosis/hyperplasia", and "bile duct inflammation" were considered as summary terms. In addition, a "combined histopathology score" representing the three individual pathological summary terms was employed in the same way as the individual summary terms for deregulated gene selection. The maximum score of the three individual summary terms, "hepatocyte cell death", "bile duct epithelial cell mitosis/hyperplasia" and "bile duct inflammation", was set as the "combined histopathology

score". Positive and negative groups were defined in different ways, attempting to increase the specificity of the gene lists obtained. These different methods were abbreviated as "S1" and "S2" samplings. For S1 sampling, the positive group was defined to consist of treated animal samples that showed a histopathology score of 2 or larger for a given summary term, and the negative (control) group consisted of those vehicle-treated animal samples that showed a score of 0 for the respective summary term. For S2 sampling, the positive group was as for S1, while the negative group consisted of those high-dose animal samples from seven studies (1RO, 3SE, 8AL, 10SG, 11OR, 12SG, 15NN) where the only pathology noted was varying degrees of hepatocyte hypertrophy (Boitier et al., 2011). These showed a score of 0 for the previously defined summary term. Using either of the S1 or S2 sampling analysis methods, the number of samples in the positive groups ranged from 25 to 36, those for the negative groups from 43 to 104.

With these sample groupings, significantly deregulated genes were selected using *t*-test and ANOVA statistics. *T*-test statistics were computed based on the logarithmized normalized expression values. The *p*-value and the Benjamini–Hochberg *q*-value were derived. The ANOVA test was performed (also based on logarithmized expression values), using as factor levels the respective histopathology scores of each summary term. Both statistics were combined with a greater or equal to 1.5 or 1.7-fold change cutoff of the medians between the positive and negative sample groups. These exact cutoffs were chosen to obtain between 400 and 700 probe sets per sample grouping and test statistic and to still maintain reasonably stringency. The resulting gene lists are provided as supplementary tables.

To visualize gene expression profiles, heat maps were generated from the normalized gene expression data. These normalized gene expression ratios were then displayed in heat maps, with the genes, shown in rows, either in a predetermined order or clustered using Euclidean as the distance metric and average linkage as the linkage parameter.

Biological analysis of gene lists. For biological interpretation of the deregulated genes, pre-selected gene lists were subjected to pathway and network analysis employing software from Ingenuity (Ingenuity Pathway Analysis (IPA) software, Ingenuity Systems, Mountain View, CA, http://www.ingenuity.com) and Genego (MetaCore™, Genego, http://www.genego.com). In addition, Entrez databases (http://www.ncbi.nlm.nih.gov/sites/entrez) including PubMed and Gene were queried for detailed gene-specific information. Using all this information the most strongly deregulated genes were categorized with respect to biochemical, cellular or organ function. Taking into account both the biochemical category and the direction of deregulation, each gene was then further assigned to a toxicological category.

Cholestasis classification based on Tx data. Tx data may be used for diagnostic or predictive classification of samples with respect to a phenotype. This assumes that gene expression deregulations in the so-called positive sample group contain a signature(s) which characterizes a particular phenotype or trait associated with these samples relative to a negative sample group. First, a classification model is trained with a training data set and then used to classify test or unknown samples by using their associated gene expression profiles (Raghavan et al., 2005). Different algorithms can be used to quantitatively describe the signature which can be a complex constellation of gene expression deregulations in the positive vs. the negative sample groups (Ringner et al., 2002; Salter and Nilsson, 2003; Man et al., 2004). In toxicology studies, properties to be modeled can include histopathological phenotypes associated already with the samples (diagnostic) or phenotypes that develop after longer treatment (predictive).

Here a classification model based on Tx data for prediction of a later developing phenotype, cholestasis, was built. A classifier for cholestasis was trained with Tx data from high dose day 2 samples from the three studies 4BA, 7SE, 14SC, as the positive sample group. These studies showed cholestasis at the late time point after high dose treatment, whereas the day 2 samples themselves were not yet associated with cholestasis. The corresponding vehicle controls were employed as the cholestasis negative sample group. This yielded five iteratively generated training and corresponding test sets (Table 2, column 1). The classifiers were calculated using Support Vector Machine (SVM) as the classifier algorithm and all genes measured on the microarray. SVM defines a hyperplane to separate samples belonging to different previously defined sample classes (Cristianini and Shawe-Taylor, 2000). Samples in this context are represented as vectors of gene expression values. The output from such a classification is affinity to any one of the input sample classes, being here the (1) cholestasis negative vehicle class and (2) the high dose day 2 samples which would show cholestasis later on if treated for a longer time. Affinity is the distance measurement of the samples to the hyperplane. Samples predicted with affinity = zero lie directly on the hyperplane, i.e. cannot be assigned to a specific class. The greater the affinity to a certain class, the clearer a sample can be said to be predicted/classified as belonging to this class. This SVM classifier was then evaluated using a randomly selected test set including one high dose day 2 sample from each study not used for training by calculating affinities to the positive and negative sample class defined by the training set.

Targeted bile acid analysis using LC-MS metabonomics. For LC-MS based metabolic profiling 50 µl of urine were mixed with 100 µl water and 50 µl serum was mixed with 100 µl acetonitrile. Samples were then centrifuged (13,000 rpm, 10 min) and transferred into LC-MS vials. LC-MS analysis was run on an Acquity UPLC System coupled to Micromass LCT Premier (ESI-TOF) spectrometer controlled by MassLynx version 4.1 software. The analytical column was an Acquity BEH C18 (dimensions: 2.1 × 100 mm, 1.7 µm) kept at 40 °C. An injection volume of 10 µl was used with a flow rate of 0.5 ml min^{-1}. Solvents were water with 0.1% formic acid (solvent A) and acetonitrile with 0.1% formic acid (solvent B) with the following gradient: 0 min 100% A, 4 min 80% A, 9 min 5% A, 10 min 5% A, 12 min 100% A. The following MS parameters were used: Ionization mode: ESI negative and ESI positive (two separate runs), survey scan mass range, 50–1000 Da; nebulization gas, 700 l h^{-1} at 450 °C; cone gas, 15–20 l h^{-1}; source temperature, 120 °C; cone voltage, 40 V, capillary voltage, 3000 V (ES+) or 2500–2800 V (ES−); LCT-W optics mode, 12000 resolution using dynamic range extension (DRE); data acquisition rate, 0.1 s with a 0.01 s interscan delay; lock spray, leucine/enkephalin (lock mass, 556.2771 *m/z*); data collection, centroid mode averaged over 10 scans. Before and after every 10th run, a blank, a test mix (MetaboMix, Waters) and another blank sample was analyzed for quality control. LC/MS raw data files were exported in the platform-independent netCDF (*.cdf) format with the MassLynx export function for further analysis. Automatic peak detection, peak alignment and peak integration was performed by XCMS. R-program version 2.6.2 (R-Foundation for statistical computing, http://www.R-project.org) and XCMS version 1.11.20 were used. The results table containing mass spectral features as mass/retention time pairs and peak integration in a tab-separated text file (*.txt) was used for further analysis. Standards of bile acids of interest (concentration 1 µg/ml) from commercial suppliers (Fluka, Sigma-Aldrich) were analyzed by LC-MS using the same instrument and the identical methods and conditions as for the specific mass/retention time pair for each bile acid. This included the following bile acids and their corresponding glycine and taurine conjugates: cholate (CA), α-muricholate (αMCA), β-muricholate (βMCA), ω-muricholate (ωMCA), deoxycholate (DCA), chenodeoxycholate (CDCA), hyodeoxycholate (HDCA), ursodeoxycholate (UDCA). The following mass/retention time pairs were used for assignment of the

bile acids in the XCMS result table ([m/z]$^-$/retention time in minutes: CA: 453.3/6.7, TCA: 514.3/6.2, GCA: 464.3/6.3, αMCA: 453.3/6.3, TαMCA: 514.3/5.5, βMCA: 453.3/6.4, TβMCA: 514.3/5.6, ΔTβMCA: 512.3/5.7, ωMCA: 453.3/6.3, DCA: 437.3/7.5, TDCA: 498.3/6.9, GDCA: 448.3/6.9, CDCA: 437.3/7.4, TCDCA: 498.3/6.8, GCDCA: 448.3/6.8, HDCA: 437.3/6.8, THDCA: 498.3/6.2, UDCA: 437.3/6.8, TUDCA: 498.3/6.4, GUDCA: 448.3/6.3). Peak integration values of the assigned bile acids from the XCMS result table were used to investigate the changes of these bile acids in urine and serum in response to drug treatment.

Results

Common findings of liver toxicity using conventional endpoints

In general, hepatotoxicity was restricted to animals treated with a high dose of 4BA, 7SE or 5ME, whereas significant changes were seen at both dose levels after treatment with 14SC. A brief summary of the characteristic histopathological and clinical chemistry changes induced by 4BA, 7SE, 5ME and 14SC is provided in Fig. 1 and in the text below.

4BA. Acute necrosis of bile duct epithelial cells was evident even after a single high dose (100 mg/kg/day) of 4BA (day 2) (Fig. 1A). These changes increased in severity after 3 days of treatment and were accompanied by bile duct hyperplasia, periportal inflammation and focal hepatocellular necrosis/hypertrophy adjacent to portal regions on day 4 (Fig. 1A). After 14 days of treatment, extensive bile duct hyperplasia with moderate periportal fibrosis/cholangiofibrosis was evident. In addition, foci of necrotic hepatocytes forming cyst-like structures filled with erythrocytes, inflammatory cells and/or necrotic hepatocytes and single cell necrosis were observed in all high dose animals at this time point (Fig. 1A). Histopathological changes on day 4 were paralleled by a rise in serum transaminases and total bilirubin (Fig. 1B).

5ME. No microscopic findings were evident on day 2 (Fig. 1A). On day 4, minimal hypertrophy of the hepatocytes was recorded in three animals receiving the high dose of 5ME (350 mg/kg/day). By day 15, marked biliary epithelial cell necrosis and bile duct inflammation accompanied by severe multifocal hepatocyte necrosis was seen in two to three individual high dose animals (Fig. 1A). Consistent with the marked inter-animal variability in this study, changes in AST, ALT, ALP and bilirubin were restricted to these animals (Fig. 1B).

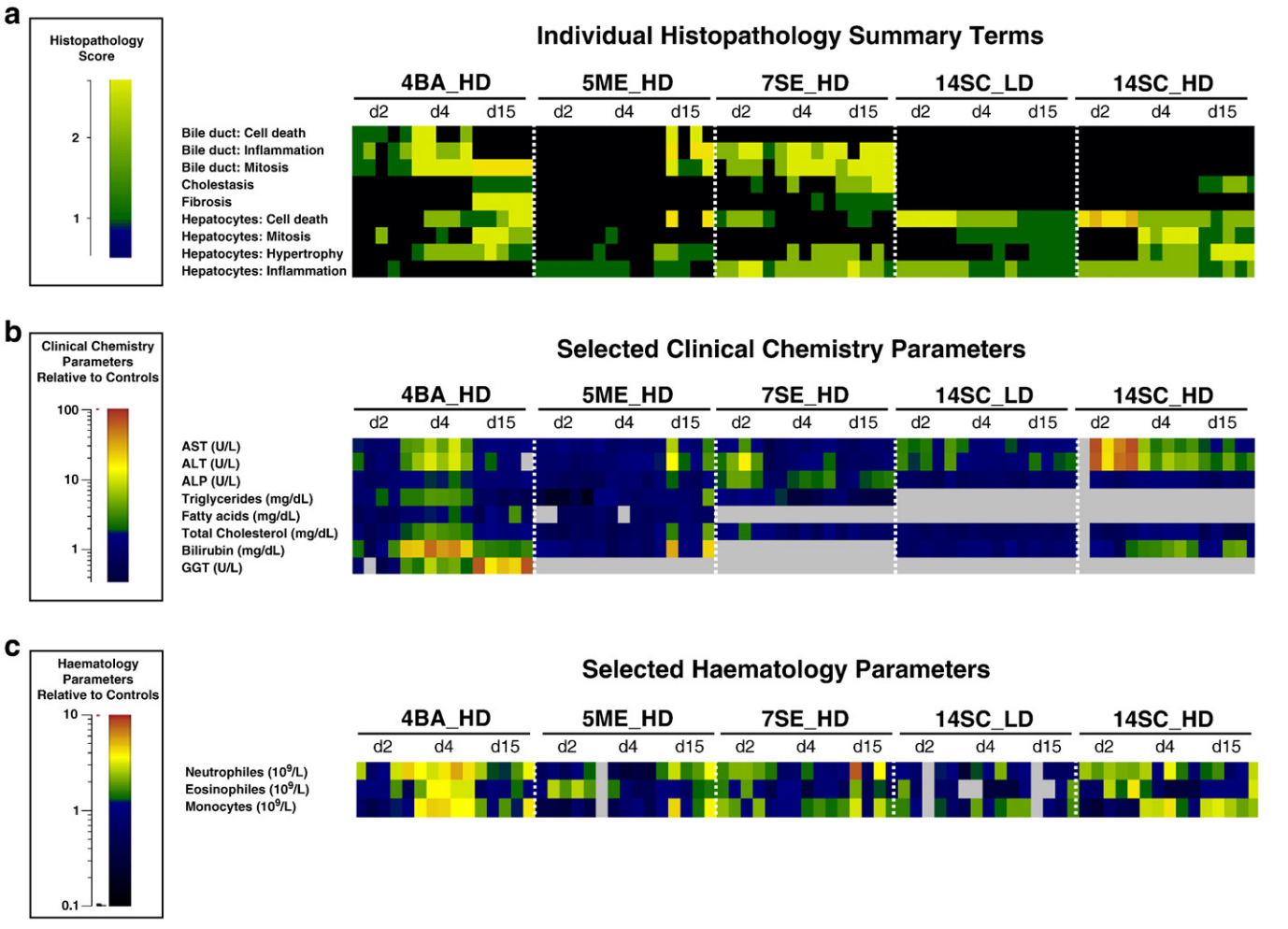

Fig. 1. Selected classical endpoints characteristic for the BDN studies. Histopathology scores (A), clinical chemistry (B) or hematology (C) parameters relative to controls were visualized in heat maps generated with Genedata Expressionist software, whereby classical endpoint parameters consistently affected by the four compounds are shown in rows and single animal for each study, dose (HD: high dose, LD: Low dose) and time point (d2, d4 and d15 corresponding to 2, 4 and 15 days after treatment including an overnight fasting period) in columns. Histological endpoints (histopathology summary terms) are shown in the upper heat map as absolute grading indicated by the histopathology score scale on the upper left. Clinical chemistry parameters measured in serum are shown in the middle panel as relative data, i.e. ratios of enzyme activity (AST: Aspartate-aminotransferase, ALT: Alanine-aminotransferase, GGT: g-Glutamyl-transferase) or metabolite levels (TGs: triglycerides, FAs: Fatty acids, Tot Chol: Total cholesterol) in the treated samples vs. the median of the matched control group. Haematology parameters including neutrophile, eosiniphile and monocyte counts are shown in the bottom heatmap as relative cell counts in the treated samples vs. the median of the matched control group.

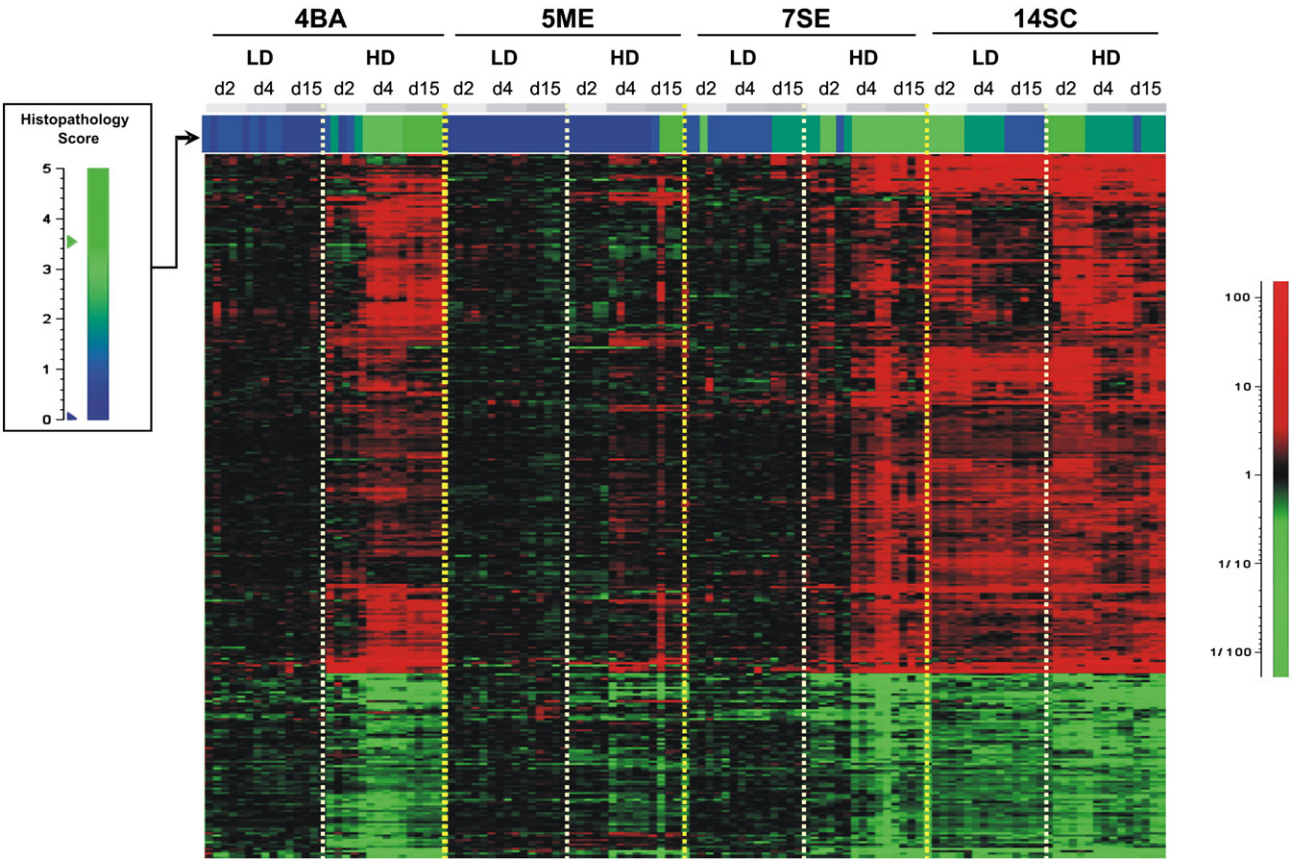

Fig. 2. Expression ratios (individual treated samples vs. median of the matched vehicle sample group (s. bottom left color scale) of the 315 genes selected with the "combined histopathology score". The genes were arranged by average linkage one-dimensional clustering with Euclidean as distance metric. LD: Low dose; HD: High dose.

7SE. Treatment with the high dose of 7SE (1000 mg/kg/day) resulted in hepatocyte necrosis, bile duct inflammation and hyperplasia in individual animals at all time points, with increasing severity related to time (Fig. 1A). After 14 days of treatment centrilobular hepatocellular hypertrophy was observed in individual animals. Cholestasis was evident in all high dose animals treated for 14 days

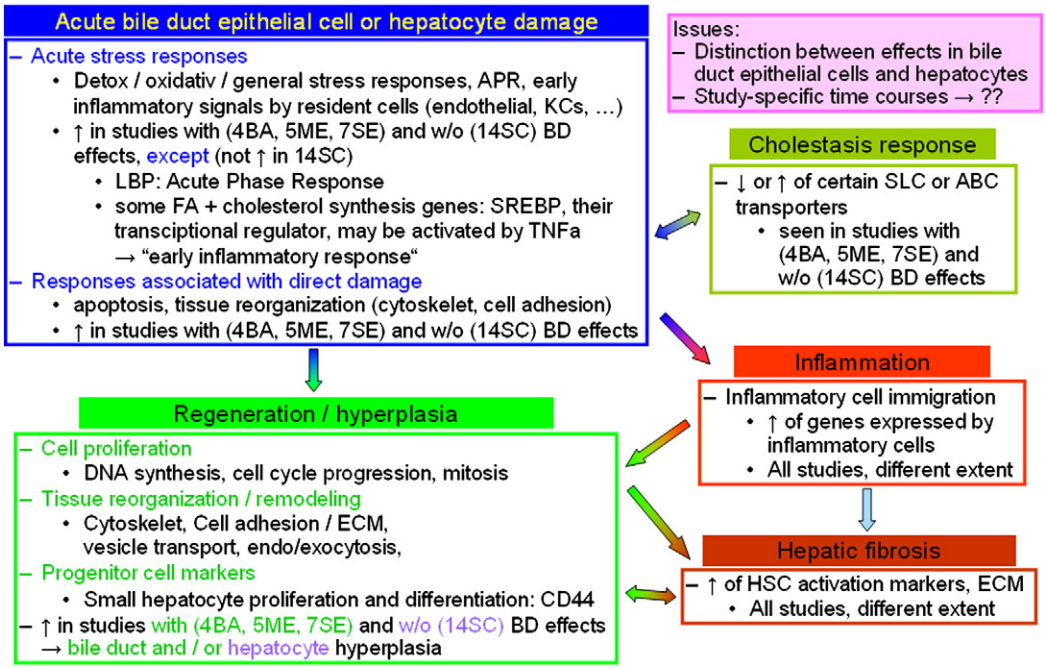

Fig. 3. Potential sequence of damage and effects derived from interpretation of the Tx liver data with respect to classical endpoint measurements. ↑ and ↓ indicate up- and downregulation of certain responses or genes. APR: Acute phase response; BD: Bile duct; ECM: Extracellular matrix; HSC: Hepatic stellate cell; KC: Kupffer cell; FA: fatty acid. Gene abbreviations: ABC: ATP-binding cassette transporter family; LBP: LPS-binding protein; SLC: Solute carrier transporter family; SREBP: Sterol regulatory element-binding protein family; TNFa: Tumor necrosis factor alpha.

Table 1
Representative examples of genes found to be characteristically deregulated in response to drugs associated with hepatobiliary toxicity.

Probe set ID	AccNo	Biochemical category	Biochemical subcategory	Gene title	Gene symbol	Entrez gene AccNo	Toxcat	Deregulation
1387011_at	NM_130741	Immunity and defense	Acute phase response	LCN2 Lipocalin 2 (NGAL Neutrophil gelatinase-associated lipocalin)	Lcn2	170496	Acute Phase Response	up
1387868_at	BF289368	Immunity and defense	Acute phase response	LBP Lipopolysaccharide (LPS)-binding protein	Lbp	29469	Acute Phase Response	up
1370080_at	NM_012580	Oxidative stress response		HO-1 Heme Oxygenase 1, microsomal	Hmox1	24451	Oxidative stress response	up
1367593_at	NM_013027	Oxidative stress response	GSH Metabolism	SEPW1 Selenoprotein W	Sepw1	25545	Oxidative stress response	up
1387818_at	NM_053736	Apoptosis	Proapoptotic	CASP4 Caspase 4 (Caspase 11)	Casp4	114555	Apoptosis	up
1384842_s_at	AI231531	Apoptosis	Proapoptotic	Fas (CD95 antigen)(TNFRSF6 TNF receptor superfamily member 6)	Tnfrsf6	246097	Apoptosis	up
1372064_at	BI296385	Immunity and defense		Similar to CXCL16 Chemokine (C-X-C motif) ligand 16	Cxcl16	497942	Inflammatory response	up
1387995_a_at	BI285494	Immunity and defense	TNF/cytokine pathway	IFITM3 Interferon induced transmembrane protein 3	Ifitm3	361673	Inflammatory response	up
1373557_at	AI145081	DNA metabolism	Replication	MCM4 Minichromosome maintenance deficient 4	Mcm4	29728	Cell cycle/proliferation—DNA Replication	up
1371074_a_at	U17565	DNA metabolism	Replication	MCM6 Minichromosome maintenance deficient 6	Mcm6	29685	Cell cycle/proliferation—DNA Replication	up
1370345_at	L11995	Cell cycle/proliferation	Cdks and cyclins	CCNB1 Cyclin B1, G2/M-specific	Ccnb1	25203	Cell cycle/proliferation—G2/M	up
1370294_a_at	U05341	Regulation of proliferation	Checkpoint	CDC20 Cell division cycle 20 (p55CDC)	Cdc20	64515	Cell cycle/proliferation—G2/M checkpoint	up
1370803_at	AF439397	Intracellular transport	Exo/endocytosis	SIP30 SNAP25 interacting protein 30 (ZWINT ZW10 interactor)	Zwint	257644	Increased intracellular transport—Exo/endocytosis	up
1388628_at	BI284430	Intracellular transport	Vesicle transport	TMED3 Transmembrane emp24 domain containing 3	Tmed3	300888	Increased intracellular transport—Vesicle transport	up
1369953_a_at	BI285141	Immunity and defense	Adaptive immunity	CD24 antigen (HSA Heat stable antigen)	Cd24	25145	Inflammatory response—Immune cell immigration	up
1368518_at	NM_012523	Immunity and defense	Adaptive immunity	CD53 Leukocyte surface antigen (Leukocyte antigen MRC OX-44)	Cd53	24251	Inflammatory response—Immune cell immigration	up
1367579_a_at	BI285434	Cytoskeleton	Microtubulin	TUBA1C Tubulin alpha 1C (TUBA6 Tubulin alpha 6)	Tuba1c	300218	Tissue reorganization—Cytoskeleton	up
1370290_at	AB011679	Cytoskeleton	Microtubulin	TUBB5 Tubulin beta 5	Tubb5	29214	Tissue reorganization—Cytoskeleton	up
1386890_at	NM_031114	Cytoskeleton	Cell morphology/motility	S100A10 (Calpactin I light chain)(p11)	S100a10	81778	Tissue reorganization—Cytoskeleton	up
1371659_at	AA891940	Cytoskeleton	Regulation	RhoC Ras homolog C (ARH9 Aplysia ras-related homolog 9) (predicted)	Rhoc	295342	Tissue reorganization—Cytoskeleton	up
1383240_at	BE110753	Cell adhesion/migration	Adhesion molecule	ITGA6 Integrin alpha-6	Itga6	114517	Tissue reorganization—Cell adhesion	up
1368819_at	AI177366	Cell adhesion/migration	Adhesion molecule	ITGB1 Integrin beta-1	Itgb1	24511	Tissue reorganization—Cell adhesion	up
1388199_at	BG376410	Cell adhesion/migration		TACSTD1 Tumor-associated calcium signal transducer 1 (EGP-314)	Tacstd1	171577	Tissue reorganization—Cell adhesion	up
1387346_at	NM_017022	Cell adhesion/migration	Adhesion molecule	ITGB1 Integrin beta-1	Itgb1	24511	Tissue reorganization—Cell adhesion to ECM	up
1388932_at	BI274917	Cell adhesion/migration	ECM	LAMA5 Laminin alpha 5	Lama5	140433	Tissue reorganization—Cell adhesion to ECM	up
1368530_at	NM_053963	Cell adhesion/migration	ECM	MMP12 Matrix metalloproteinase 12 (MME Macrophage metalloelastase)	Mmp12	117033	Tissue reorganization—Cell adhesion to ECM	up
1367681_at	NM_022523	Cell adhesion/migration	Regulation	CD151 Platelet endothelial tetraspan antigen 3	Cd151	64315	Hepatic fibrosis—Migration of activated HSCs	up
1367709_at	NM_017125	Cell adhesion/migration	Adhesion molecule	CD63 antigen (AD1 antigen)	Cd63	29186	Hepatic fibrosis—Migration of activated HSCs	up
1387952_a_at	AF065147	Cell adhesion/migration	ECM/Cell adhesion molecule	CD44 antigen (ECMR-III Extracellular matrix receptor-III)	Cd44	25406	Hepatic fibrosis—Proliferation of small hepatocytes upon hepatocyte damage, migration of activated HSCs	up
1367712_at	NM_053819	Cell adhesion/migration	ECM	TIMP1 Tissue inhibitor of metalloproteinase 1	Timp1	116510	Hepatic fibrosis	up
1368609_at	NM_017047	Membrane transport/Biotransformation	Bile acid transport/Phase III	NTCP Sodium/taurocholate cotransporting polypeptide, hepatic (SLC10A1)	Slc10a1	24777	Cholestatic response—reduced bile acid uptake from plasma into hepatocytes	down
1369440_at	NM_130414	Steroid metabolism/Membrane transport	Regulation	ABCG8 ATP-binding cassette sub-family G (WHITE) member 8 (Sterolin 2)	Abcg8	155192	Cholestatic response—reduced biliary sterol excretion	down

Table 1 (*continued*)

Probe set ID	AccNo	Biochemical category	Biochemical subcategory	Gene title	Gene symbol	Entrez gene AccNo	Toxcat	Deregulation
1369455_at	NM_053754	Steroid metabolism/ Membrane transport	Regulation	ABCG5 ATP-binding cassette sub-family G (WHITE) member 5 (Sterolin 1)	Abcg5	114628	Cholestatic response—reduced biliary sterol excretion	down

Probe set ID: Identification number given on the Affymetrix Microarray.
Acc No: Public gene accession number (http://www.ncbi.nlm.nih.gov/sites/entrez?db=nuccore).
Biochemical category: One to two biochemical mean categories to which the gene was assigned.
Biochemical subcategory: One of several biochemical subcategories each per main category to which the genes was assigned.
Gene Title: Title/Name of the gene preceded by the gene symbol.
Gene symbol: official gene symbol listed in Entrez Gene (http://www.ncbi.nlm.nih.gov/sites/entrez).
Entrez Gene AccNo: official Accession number for the Entrez Gene database (http://www.ncbi.nlm.nih.gov/sites/entrez).
Toxicological category: Category with respect to (toxicological) phenotype or pathway to which the gene was assigned.
Deregulation: Main direction of deregulation in the BDN study samples.

(Fig. 1A). ALP and total bilirubin were increased at all time-points, whereas elevated levels of AST and ALT were only seen on days 2 and 4 (Fig. 1B).

14SC. Hepatic lesions induced by 14SC were characterized by centrilobular hepatocellular necrosis, vacuolation, hypertrophy and signs of inflammation (infiltration of mononuclear cells) and regeneration, with increasing severity related to dose. Hepatocellular necrosis, accompanied by a dose-dependent increase in serum transaminases, was most severe on day 2 and declined on days 4 and 15 (Fig. 1A and B). The time-dependent decline in severity of hepatocellular necrosis was paralleled by increasing hepatocellular vacuolation and hypertrophy as well as regeneration and mitosis (Fig. 1A). An increase in total bilirubin was seen in high dose animals at all time points (Fig. 1B). On day 15, cholestasis was observed in animals treated at a dose of 1120 mg/kg/day 14SC.

Thus, a common feature of all four compounds was the induction of hepatobiliary toxicity, evidenced by bile duct epithelial cell necrosis and hyperplasia and/or increased bilirubin and cholestasis, in addition to hepatocellular necrosis, regeneration and hypertrophy, and inflammation within the bile ducts and/or parenchyma (Fig. 1A and B). However, both severity and time of manifestation of biliary vs. hepatocellular changes varied between compounds. For instance, damage to the biliary epithelium in response to treatment with 4BA was seen before hepatocellular necrosis was evident, whereas both bile ducts and hepatocytes appeared to be targeted in parallel after treatment with 7SE and 5ME (Fig. 1A). In contrast, treatment with 14SC led to early damage of hepatocytes, with cholestasis developing later on (Fig. 1A). Increases in granulocyte and/or monocyte numbers paralleled the acute hepatobiliary damage likely reflecting a general inflammatory response (Fig. 1C).

Tx data in relation to drug-induced hepatobiliary injury

The more detailed histopathological terms used by the individual study pathologists were merged into summary terms, representing major toxicological phenotypes of the liver, and are related to those proposed by Cattley and Popp (2001) to allow more straightforward grouping of samples for item selection. Hepatocyte cell death, bile duct inflammation and bile duct epithelial cell mitosis/hyperplasia were the major distinguishing pathologies observed in the four studies reported here (Fig. 1A). The aim of data analysis across all compounds (cross compound analysis) of Tx liver data was to identify gene groups representing pathways and/or functions involved in these three pathologies. As described above, pairs of sample groups positive and negative for these pathologies were assembled according to predefined criteria with respect to histopathological summary term scores.

The genes were ranked based on *p*- or *q*-values from ANOVA or *t*-tests. Genes selected with a certain *p*- or *q*-value cutoff were then additionally subjected to a ratio cutoff calculated as median deregulation between the corresponding positive and negative sample groups. Exact cutoffs were chosen to obtain ca. 400–700 probe sets per sample grouping, based on ANOVA *p*-value cutoffs of 10^{-4} or 10^{-5}, or a *t*-test *q*-value cutoff of 10^{-2}, combined with 1.5 or 1.7-fold or greater deregulation between treated and control sample groups. These statistical gene selections then resulted in 400 to 550 probe sets after excluding complete unknowns (supplementary online tables). Since these gene groups showed significant overlap, even between the two negative group sampling methods, a “combined histopathology score” was created from the three summary terms—hepatocyte cell death, bile duct inflammation, and bile duct epithelial cell mitosis/hyperplasia—setting the maximum score from each of the three single pathological summary terms. An ANOVA *q*-value cutoff of 10^{-4} combined with a 1.7-fold median ratio cutoff between this “combined histopathology score”—positive and negative sample groups yielded 315 probe sets, after subtracting those encoding unknown transcripts. The gene expression profiles of genes selected with the “combined histopathology” term are shown in Fig. 2, illustrating a similar dose, time and sample dependency of the magnitude of gene expression deregulations as the effects on conventional parameters indicated in the heatmap in Fig. 1. Corresponding gene lists obtained with these criteria are available as supplementary tables. Overall datasets have been submitted to the EBI and are being curated via the ISA infrastructure (Rocca-Serra et al., 2010). They will be made accessible via the multi-omics BioInvestigation Index database (http://www.ebi.ac.uk/bioinvindex/browse_studies.seam).

For biological interpretation of the deregulated genes obtained with the three individual summary terms and the “combined histopathology” term, two pathway software tools were used. These indicated, amongst others, liver hyperplasia, liver damage and liver hepatitis as significantly enriched Tox functions (IPA), and apoptosis, cell cycle control, amino acid and nucleotide metabolism, and cyto/chemokines as significantly enriched cell processes (Metacore). However, since these tools provided information for only about 50% of the deregulated genes, a gene by gene approach was also applied, especially to those genes represented by most of these gene groups. The cellular or organ function of the protein encoded by this gene, the direction of deregulation, and available knowledge about deregulation of the expression of a gene under certain conditions, stresses, or pathological situations was considered. This revealed altered expression of genes involved in acute phase response, response to inflammation and oxidative stress, apoptosis, cell proliferation and tissue reorganization, fibrosis and response to cholestasis (Fig. 3). The gene by gene approach confirmed the pathways and functions revealed by the pathway software's (data not shown) yet added more detail and allowed better overall interpretation. In conjunction with the observed classical endpoints, interpretation of liver Tx data led to a detailed postulated sequence of events in drug induced liver

injury and response to damage. This was characterized by altered expression of (1) genes involved in acute damage response reflecting acute biliary epithelial cell and/or hepatocyte necrosis, (2) solute carriers (*SLC*) and ATP-binding cassette (ABC) transporters suggestive of cholestasis, (3) mediators of inflammation indicative of an inflammatory response, (4) progenitor cell markers and genes involved in cell proliferation and tissue reorganization reflecting tissue regeneration, and (5) hepatic stellate cell activation markers and extracellular matrix components symptomatic of fibrosis (Fig. 3). Representative genes associated with this sequence of events (Table 1) will be reviewed in the discussion section.

Although Tx data revealed common gene expression changes in the liver which allowed us to define a potential damage sequence at a mechanistic level in accordance with histopathological observations, a distinction between expression changes arising from the hepatocytes vs. biliary epithelial cells was not possible. Thus, immunolocalization studies were conducted for selected genes involved in acute phase and inflammatory responses (*NGAL/lipocalin 2*), cell proliferation/regeneration (*PCNA*) and tissue reorganization/fibrosis (*Timp-1*). In line with the histopathological observations, *PCNA* was detected in both hepatocytes and bile duct epithelial cells after treatment with 4BA and 7SE, whereas positive *PCNA* staining was restricted to hepatocytes following treatment with 14SC (Fig. 4a), providing further molecular support for the exclusive hepatocellular vs. the mixed hepatocellular/biliary epithelial effects of 14SC and 4BA/7SE, respectively. Similarly, increased expression of *NGAL/lipocalin2* was evident predominantly within the liver parenchyma, but not in biliary epithelial cells following treatment with 14SC (Fig. 4b), consistent with the absence of bile duct effects. In contrast, both hepatocytes and biliary epithelial cells stained positive for *NGAL/lipocalin2* in response to 4BA and 7SE (Fig. 4b). As expected, increased Timp-1 was associated with areas of fibrosis following treatment 4BA and 7SE (Fig. 4c).

Deregulation of hypertrophy associated genes

In addition to hepatocyte and bile duct epithelial cell degeneration/regeneration and inflammation, hepatocellular hypertrophy was recorded as a comparatively minor finding in response to treatment with 4BA, 5ME, 7SE and 14SC. In contrast, hepatic effects of a range of other compounds studied within the frame of the InnoMed-PredTox project were characterized by hypertrophy in the absence of major histopathological changes (Boitier et al., 2011; Suter et al., 2011), and thus gene expression changes seen in response to these compounds are assumed to be linked to hypertrophy. For gene selection, samples obtained from studies showing hypertrophy only were divided into two study sets based on the likely underlying mechanisms for hypertrophy. These two study sets represented either a Xenobiotic metabolism (XME) phenotype, characterized predominantly by endoplasmic reticulum

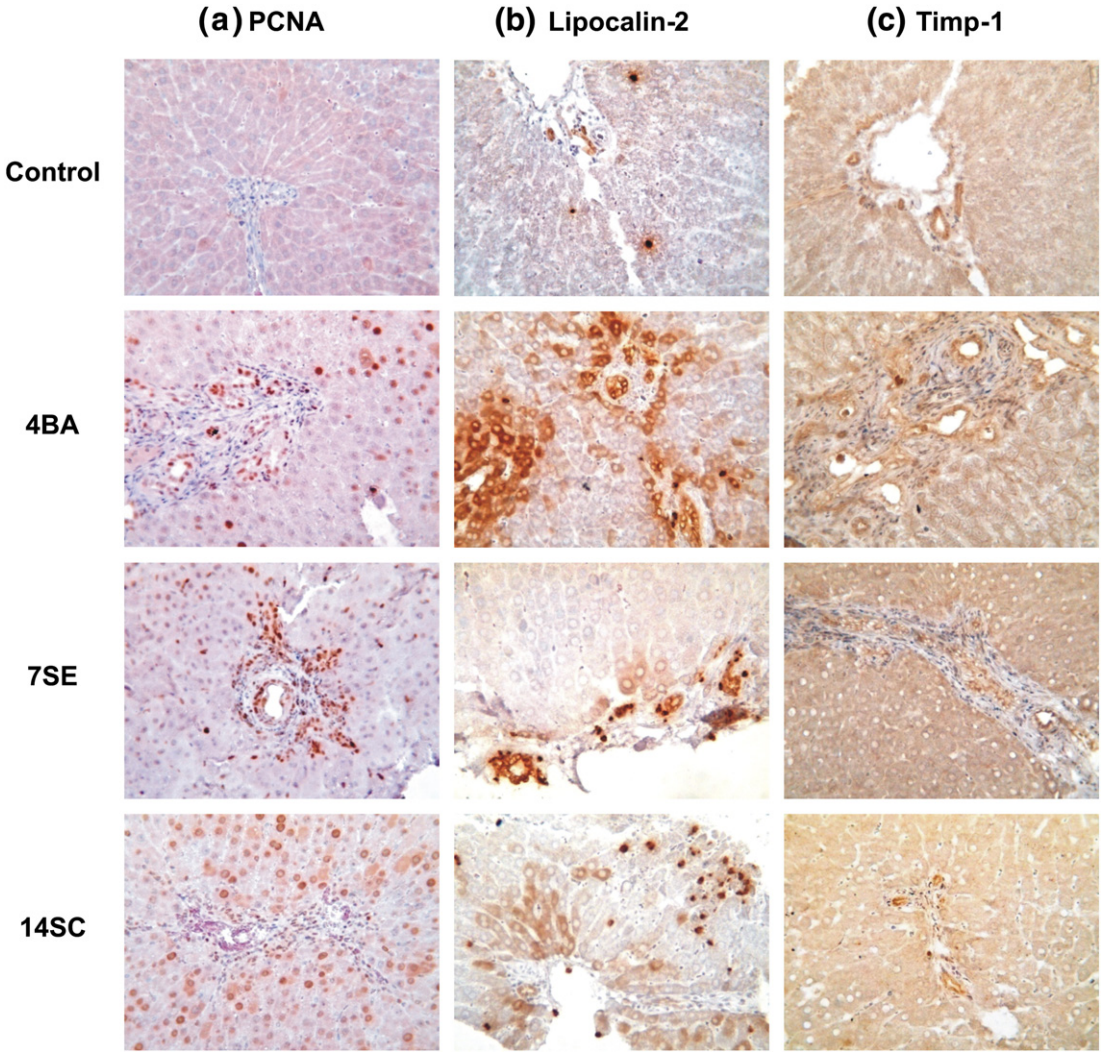

Fig. 4. Representative photomicrographs showing immunolocalization of key markers of (a) proliferation/regeneration (PCNA), (b) acute phase/inflammatory response (NGAL/lipocalin-2), and (c) tissue reorganization/fibrosis (Timp-1) after treatment with 4BA, 7SE and 14SC.

(ER) proliferation, or a "PP" phenotype with peroxisome proliferation (Boitier et al., 2011). Consolidated gene lists characteristic for the XME or PP phenotype, which included genes representing xenobiotic metabolism in general or fatty acid metabolism, respectively (Boitier et al., 2011), were used to visualize expression of hypertrophy associated genes in samples of studies showing hepatobiliary toxicity in addition to hypertrophy. Hypertrophy associated genes were generally induced before appearance of hypertrophy during the time course of studies showing hepatobiliary toxicity (Fig. 5). Concerning general XME gene induction (Fig. 5a), studies 4BA, 5ME and 14SC showed patterns similar to the studies with XME phenotype (Boitier et al., 2011). 5ME clearly induced genes encoding fatty acid oxidation enzymes (Fig. 5b), similar to the PP studies (Boitier et al., 2011). Based on the gene lists analyzed in this context, study 7SE showed a hypertrophy phenotype different from the other studies with hepatobiliary effects (Fig. 5 and data not shown).

Prediction of drug-induced cholestasis based on TX data

Three studies, 4BA, 7SE, 14SC, showed cholestasis, mainly at the late time point after high dose treatment. To investigate the potential of using Tx data for earlier prediction of this specific toxic endpoint, a classifier for cholestasis was "trained" with Tx data from high dose day 2 samples which were not yet associated with cholestasis, as the positive sample group, and the corresponding vehicles as the cholestasis negative sample group. The classifier was then evaluated using a randomly selected test set including one high dose day 2 sample from each study not used for training. This yielded five iteratively generated training and corresponding test sets (Table 2, column 1). The predictions of different test set combinations (day 2 high dose) with correspondingly different classifiers all showed positive affinities, mostly >0.5, to the correct class, except for 7SE animal #15, which showed an affinity of 0.36 for the cholestasis-negative vehicle class. Thus the predictions were all correct, i.e., predicted as 'day 2 high dose showing cholestasis later on', except for 7SE animal #15, which was predicted as "vehicle" (Table 2).

Targeted bile acid analysis based on global Mx by LC-MS

All drug candidates investigated here induced hepatobiliary toxicity, evident by bile duct epithelial cell necrosis and/or increased bilirubin and cholestasis, in addition to hepatocellular changes. However, whereas 14SC induced hepatocyte damage only, livers of rats treated with 4BA and 5ME also showed severe injury of the bile duct epithelium. To obtain further insight into the mechanisms involved and to test the utility of individual bile acids as markers of different types of hepatobiliary toxicity, the effect of 4BA, 5ME and 14SC on a range of conjugated and unconjugated bile acids in urine and serum was investigated using metabonomics LC/MS. From the different bile acids examined and described in the methods, only those bile acids are summarized which could be detected and which showed the most significant compound related changes in urine and serum. Treatment with 14SC resulted in a marked increase of cholic acid, an unconjugated bile acid, in urine, in addition to some minor changes of conjugated bile acids in serum and urine (Table 3). In contrast, conjugated bile acids, including taurocholic acid and glycocholic acid, were substantially increased in both serum and urine after treatment with 4BA (Table 3), along with a comparatively small increase in the levels of unconjugated bile acid. These were paralleled by a significant rise in serum transaminases, ALP and bilirubin, indicative of the hepatobiliary toxicity of BA, but were much more pronounced (Table 3). Although few statistically significant changes were observed in response to 5ME due to the large inter-animal variability in this study, a dramatic rise in the levels of conjugated bile acids accompanied by increased levels of cholic acid was seen in those individual high dose animals that exhibited marked biliary epithelial cell necrosis and severe multifocal hepatocyte necrosis after 14 days of treatment. Interestingly, these changes were preceded by a marked increase in cholic acid along with moderate effects on conjugated bile acids on day 4.

Discussion

Potential damage sequence in the liver based on Tx data

As indicated in the Results section, analysis of Tx data revealed common gene expression changes (representative examples for genes are shown in Table 1) in the livers of rats showing damage to the hepatobiliary tract, which allowed us to define a potential sequence of events at a mechanistic level in accordance with histopathological observations. This included molecular changes reflecting acute damage to bile duct epithelial cells or hepatocytes, characterized by early stress responses and cell death (apoptosis/necrosis), regenerative processes, inflammation with inflammatory cell immigration, and finally fibrotic processes and cholestasis (Fig. 3).

In the present study, upregulation of genes involved in acute stress responses, including acute phase response (APR) genes, represented by *LCN2 (lipocalin 2)* (Sunil et al., 2007) and *LBP (lipopolysaccharide (LPS)-binding protein)* (Schumann and Zweigner, 1999), were interpreted as a response to acute damage of bile duct epithelial cells or hepatocytes. Whereas *LCN2* is suggested to be important in restoring tissue homeostasis following LPS-induced injury (Sunil et al., 2007), an enhancing role in the inflammatory response has been reported for *LBP* in the context of bile duct ligation (Minter et al., 2005), a condition which induces extrahepatic cholestasis. Interestingly, *LBP* was mostly upregulated after treatment with 4BA and 7SE, which resulted in marked injury to the biliary epithelium. Thus, whether upregulation of such acute stress response genes serves to protect from or rather promotes inflammation may depend on the extent and persistence of increased expression.

Several of the deregulated genes, such as *HO-1 (heme oxygenase 1)* and *SEPW1 (selenoprotein W)* which are associated with oxidative or free radical stress and reported to have antioxidant, protective functions (Bauer and Bauer, 2002; Jeong et al., 2004; Loflin et al., 2006), may be linked to acute tissue injury or inflammation.

Genes involved in the initiation and execution of cell death, including *CASP4 (Caspase 4 = Caspase 11)* and *FAS antigen* (Malhi et al., 2006), were found to be expressed at increased levels in the present study. In addition, deregulation of genes with functions in tissue organization, such as genes encoding cytoskeletal and cell adhesion molecules, e.g. *S100A10, RhoC (Ras homolog C)*, various *tubulins*, *integrins* and *TACSTD1 (tumor-associated calcium signal transducer 1)*, may also have been associated with activation of cell death. Early apoptotic events are reported to be accompanied by stabilization of the microtubule cytoskeleton and translocation of organelles to the microtubule organizing center leading to death receptor endocytosis, mitochondrial and lysosomal permeabilization, calcium release from the endoplasmic reticulum and fragmentation of the Golgi apparatus (Aslan and Thomas, 2009). Upregulation of *integrins* in response to drug treatment might be interpreted as a survival signal as part of an adaptive response (Stupack and Cheresh, 2002).

An early inflammatory response, including increased levels of cytokine pathway mRNAs, accompanied these acute damage effects, e.g. upregulation of mRNAs encoding *IFITM3 (interferon induced transmembrane protein 3)* and *CXCL16 (chemokine ligand 16)*, probably by Kupffer cells (KC) or endothelial cells (Xu et al., 2005). Upregulation of some fatty acid and cholesterol synthesis genes may also have been a component of this early inflammatory response, since expression of *sterol regulatory element-binding proteins* (*SREBP*s), which act as transcription factors for these genes, is enhanced by *tumor necrosis factor alpha (TNF*α) signaling (Fon Tacer et al., 2007).

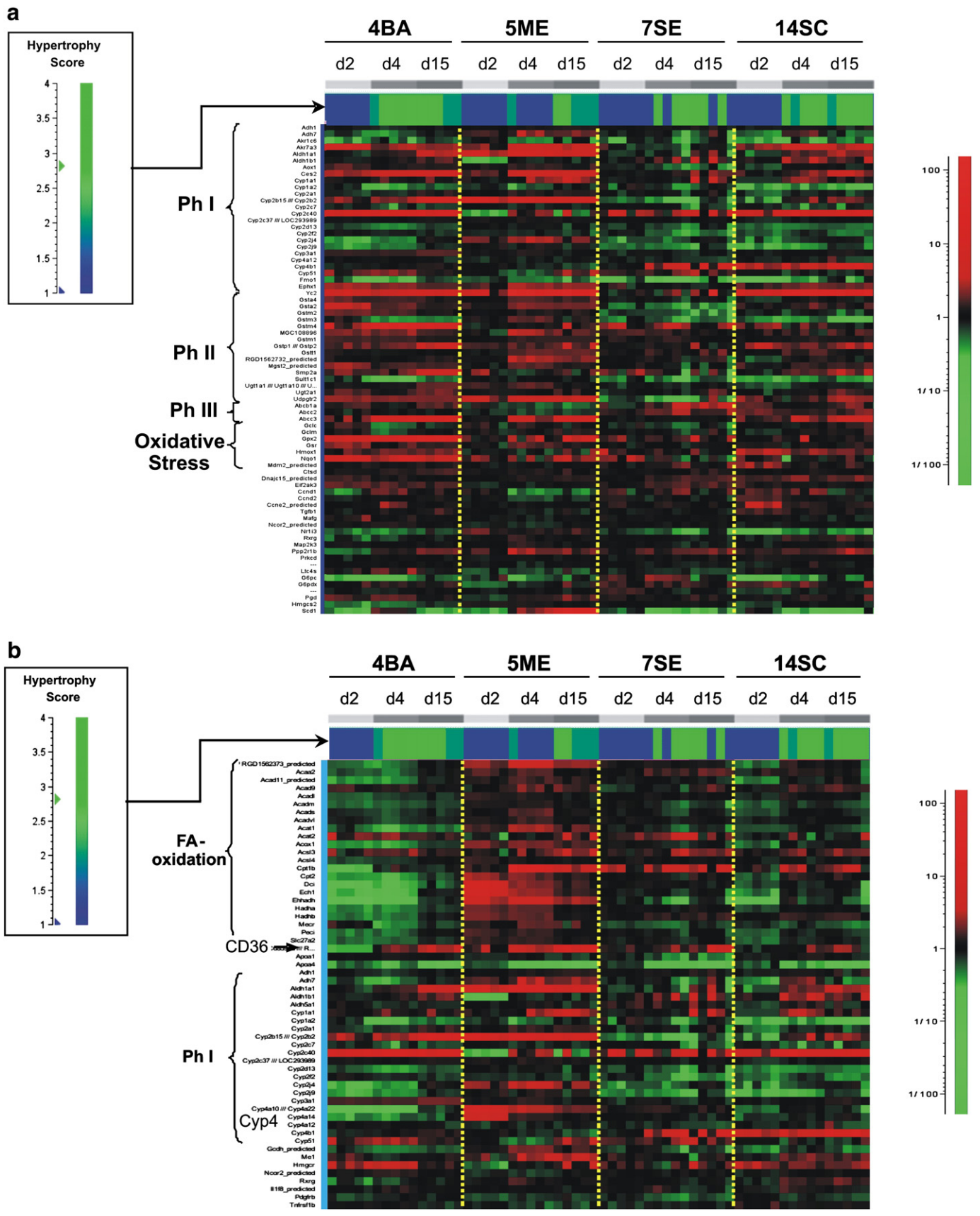

Fig. 5. Expression ratios (single treated samples vs. median of the matched vehicle sample group, bottom left color scale) of genes representing xenobiotic metabolism in general (a) and fatty acid metabolism characteristic for the PxP phenotype (b), in the samples indicated above the heatmap. The genes are ordered by functions, which are given on the left. The samples are ordered by time point of necropsy (d2, d4, d15), study and study group, as depicted at the top of the heat map. The colored lane below the time point display indicates the Hypertrophy (HYP) score in each sample according to the scale given on the left. Ph I, II, III: Biotransformation Phase I, II, and III genes; oxStress: Oxidative stress responses genes; Fa oxidation: Genes encoding fatty acid oxidation enzymes.

Table 2
Classification of the high dose day 2 liver expression profiles of the samples indicated in the 2nd column with respect to development of cholestasis at later time points. The output from classification is affinity to either the cholestasis-negative or vehicle class (column 4) or the positive class (column 3) corresponding to high dose day 2 samples after treatment with compound inducing cholestasis later on. Classification was performed using SVM as classifier with a linear kernel and a penalty of 10. Only the transcripts with at least 50% valid values were used.

Test set	Animal no.	Affinity to the sample class showing cholestasis later on	Affinity to the vehicle class
1	4BA_A14	0.76	
	7SE_A11	0.34	
	14SC_A14	0.96	
2	4BA_A11	1.15	
	7SE_A12	0.5	
	14SC_A15	1.53	
3	4BA_A11	1.25	
	7SE_A15		0.36
	14SC_A14	1.26	
4	4BA_A11	0.76	
	7SE_A11	0.35	
	14SC_A12	1.04	
5	4BA_A14	0.77	
	7SE_A12	0.51	
	14SC_A13	0.76	

Induction of genes involved in DNA synthesis and cell cycle progression observed in response to drug treatment, represented by *MCM4 (minichromosome maintenance deficient 4)*, *MCM6*, *CCNB1 (cyclin B1)*, and *CDC20 (cell division cycle 20)* (Harper and Brooks, 2005), is likely to be linked to regenerative processes following the drug-induced injury to bile duct epithelial and/or parenchymal cells (Fausto and Campbell, 2003). The upregulation of genes with functions in cytoskeletal organization and cell adhesion as mentioned above, in vesicle transport (e.g. *TMED3 (Transmembrane emp24 domain containing 3)*), and in endo/exocytosis (e.g. *SIP30 (SNAP25 interacting protein 30)*), and genes playing a role in extracellular matrix formation and maintenance (e.g. *MMP12 (Matrix metalloproteinase 12)* and *LAMA5 (Laminin alpha 5)*) may also contribute to regeneration, as increased expression of genes or proteins related to these processes was previously shown in liver regeneration models (Nakamura et al., 1994; White et al., 2005; Yuan et al., 2009). Similarly, increased expression of progenitor cell markers (e.g. *CD44*), indicating recruitment of precursor cells for tissue regeneration (Kon et al., 2006), may play a role in the regenerative hyperplasia observed in our studies.

Increased levels of transcripts encoding genes and markers expressed by inflammatory cells, e.g. *CD24* and *CD53* antigens, are most likely a result of inflammatory cell infiltration, which was observed histologically in both the biliary epithelium and liver parenchyma in parallel or subsequent to the appearance of necrosis.

Increased expression of previously described Hepatic stellate cell (HSC) activation markers, including *CD151 platelet endothelial tetraspan antigen 3* and *CD63 antigen* (Mazzocca et al., 2002) and components/regulators of the extracellular matrix, e.g. *TIMP1 (tissue inhibitor of metalloproteinase 1)*, which are reported to be expressed in activated HSCs (Murphy et al., 2002), indicate development of hepatic fibrosis. This is in line with the fibrosis seen in response to 4BA and 7SE as well as in individual animals treated with 5ME. As HSCs are central mediators of hepatic fibrosis (Murphy et al., 2002), it is interesting to note that these genes were also found to be increased after treatment with 14SC, suggesting that activation of HSCs and hepatic fibrosis may develop after prolonged treatment. Since some of the responses seen after 14SC treatment appeared to be transient, with respect to both classical endpoints and gene expression, other signals required for development of fibrosis may have been missing or counter regulatory pathways may have been activated after treatment with this compound.

The *ABCG5* and *ABCG8* membrane transporters of the ABC family, which are localized in the canalicular membrane of hepatocytes, mediate cholesterol secretion into bile. They have both been found to be downregulated at the mRNA level during cholestasis induced by bile duct ligation (Kamisako and Ogawa, 2005). Similarly, the *SCL10A1* membrane transporter, also known as *NTCP sodium/taurocholate cotransporting polypeptide*, a basolaterally located Na(+)/bile acid cotransporter of the hepatocyte, has been reported to be downregulated in estrogen-mediated cholestasis (Geier et al., 2003). The expression levels of all three genes encoding these transporters were decreased after treatment with 4BA, 7SE and 14SC, and are likely to be associated with the cholestasis observed histologically. The 5ME study, for which the pathologist did not report cholestasis, showed a weaker but detectable decrease of these genes, especially in the two most affected animals. Downregulation of these transporters may be a

Table 3
Levels of individual bile acids in urine and serum after high dose treatment with 14SC, 4BA and 5ME relative to controls. For comparison, drug induced changes in liver enzymes and bilirubin relative to controls are included. Data are presented as mean ± SD. Statistically significant changes are indicated by $^{*}p<0.05$, $^{**}p<0.01$, $^{***}p<0.001$ (ANOVA + Dunnett's post hoc test).

	14SC (HD)			4BA (HD)			5ME (HD)		
	Day 2	Day 4	Day 15	Day 2	Day 4	Day 15	Day 2	Day 4	Day 15
Urine									
CA	17.5 ± 12.8*	303 ± 494	45.1 ± 19.2**	1.3 ± 0.9	101 ± 110	20.9 ± 20.2**	12 ± 3.1***	536 ± 618	1870 ± 2748
GCA	6.4 ± 4.1*	21.0 ± 21.8	3.7 ± 2.9	2.2 ± 1.1	4738 ± 2843**	49.7 ± 19.0***	9.5 ± 6.2*	26.2 ± 24.2	3669 ± 6545
TCA	6.5 ± 3.1**	28.1 ± 18.3**	5.2 ± 2.2**	1.2 ± 0.7	554 ± 297***	5.4 ± 2.4***	1.1 ± 0.9	14.0 ± 6.1**	88107 ± 134282
TβMCA	4.5 ± 2.1**	6.9 ± 8.4	6.2 ± 5.4	1.0 ± 0.4	5876 ± 3734**	37.4 ± 27.1**	12 ± 8.6*	5.1 ± 4.1	15294 ± 21632
ΔTβMCA	< LOQ	< LOQ	< LOQ	3.6 ± 1.7*	8605 ± 4914***	25.3 ± 21.5*	1.7 ± 0.8	1.2 ± 0.4	97926 ± 151643
Serum									
CA	1.5 ± 0.2	5.2 ± 2.9**	1.6 ± 0.9	0.7 ± 0.6	2.6 ± 0.9*	1.0 ± 0.4	2.6 ± 2.1	0.6 ± 0.3	1.5 ± 0.9
GCA	0.4 ± 0.3	0.4 ± 0.1*	2.3 ± 0.9**	10.3 ± 11.3	17.8 ± 11.2**	7.3 ± 3.4***	0.8 ± 0.7	0.3 ± 0.2**	4.5 ± 4.0
TCA	9.4 ± 2.9***	11.3 ± 5.8**	2.7 ± 0.9**	95.4 ± 140.7	720 ± 231***	21.4 ± 8.8***	< LOQ	< LOQ	< LOQ
TβMCA	1.4 ± 0.8	1.3 ± 0.9	1.9 ± 0.8	71.9 ± 104.1	520 ± 128***	24.5 ± 9.7***	0.8 ± 0.3	0.3 ± 0.1	0.7 ± 0.2
ΔTβMCA	5.3 ± 2.6**	5.1 ± 1.7***	1.1 ± 0.3	55.3 ± 83.11	546 ± 80***	28.8 ± 11.5***	1.1 ± 0.7	0.5 ± 0.2	2.7 ± 2.9
ALT	48.3 ± 20.6***	5.7 ± 1.8***	2.9 ± 1.1**	1.6 ± 1.0	7.8 ± 2.4***	1.5 ± 0.4**	0.9 ± 0.1	1.3 ± 0.3	4.3 ± 4.9
AST	51.0 ± 24.3***	3.7 ± 1.5**	1.7 ± 0.4*	1.7 ± 1.1	5.9 ± 2.9**	1.4 ± 0.2**	1.0 ± 0.1	1.1 ± 0.3	2.8 ± 2.7
ALP	1.0 ± 0.2	1.3 ± 0.1	0.9 ± 0.2	1.0 ± 0.2	1.8 ± 0.2***	1.2 ± 0.2*	0.9 ± 0.2	0.9 ± 0.2	1.3 ± 0.6
Bilirubin	1.5 ± 0.6***	3.5 ± 1.0	2.5 ± 1.5	6.5 ± 10.4	35.5 ± 13.7***	2.8 ± 0.4***	1.2 ± 0.3	0.8 ± 0.2	10.7 ± 13.3

HD: high dose, LD: low dose, LOQ: limit of quantification, CA: cholate, GCA: glycocholate, TCA: taurocholate, TβMCA: tauro-β-muricholate, ΔTβMCA: unsaturated tauro-β-muricholate, ALT: alanine aminotransferase, AST: asparate aminotransferase, ALP: alkaline phosphatase.

feedback response to reduced bile flow since decreased levels of *ABCG5/ABCG8* and *NTCP* are likely to result in reduced biliary sterol excretion and bile acid uptake from plasma into hepatocytes, respectively, thereby reducing overall bile formation. Interestingly, the transporter mRNA downregulation was detectable before development of histologically observable cholestasis. Therefore, either the changes in bile flow influenced transporter gene expression before being morphologically detectable, or instead of being a response to defects in bile flow, the transporters may have been downregulated in parallel to functional perturbations in the hepatocyte, thereby playing a direct role in bile flow defects.

In summary, common liver gene expression changes observed in response to drug-induced hepatobiliary injury revealed a potential damage sequence in accordance with histopathological observations. Acute damage to biliary epithelial cells or hepatocytes was indicated by early stress responses and altered expression of genes associated with apoptosis and/or necrosis. In addition to a general APR, some of the induced transcripts may be indicators of certain forms of primary damage, e.g. oxidative or free radical stress. An early inflammatory response, including increased levels of cytokine pathway mRNAs, accompanied these acute damage effects. Depending on the strength and duration of these acute responses, these could either help repair or even exacerbate tissue damage. Following this early injury, regenerative processes, indicated by de- (mostly up-) regulated genes functioning in cell cycle progression and cell morphology, were switched on. The degeneration/regeneration processes were accompanied by inflammation with inflammatory cell migration. Increased expression of HSC activation markers probably leads to fibrotic changes observed in some of the studies at the later time point. Finally, downregulation of certain membrane transporter genes appears to be mechanistically linked with cholestasis, as seen following treatment with 4BA, 7SE, and 14SC. Importantly, altered expression of these genes in response to 4BA, 7SE, and 14SC was observed before cholestasis became apparent, suggesting that the minor downregulation seen following treatment with 5ME represent an early indication of the development of cholestasis after prolonged treatment.

Prediction of cholestasis based on Tx data

Earlier prediction of the potential of a drug to induce toxicity following long-term administration would greatly facilitate the drug development process by helping to rank drug candidates or shape the safety testing program (Blomme et al., 2009). To test if early prediction of a pathology that develops later is possible even based on a limited number of studies. A gene expression profile-based prediction model was developed for cholestasis, which was observed after 14 days of treatment with 4BA, 7SE, and 14SC. A training set of all day 2 samples per study representing gene expression changes induced before appearance of cholestasis was assembled as a positive class, together with the corresponding vehicle samples as the cholestasis-negative class. One sample per study was withheld and used as a test set to evaluate the predictive outcome of the classifier, calculated with the training set. The test set classifications looked promising with respect to cholestasis prediction accuracy, since only 1 of 15 positive group samples (predicted in groups of 3 in five iterations) was wrongly classified as vehicle, i.e. cholestasis-negative. Since the training set was associated with toxicities other than cholestasis, this result should be appreciated as an indication that early prediction of a subsequent toxicological phenotype might be possible, although this will require further testing with more suitable and larger data sets not available within this project. Within this context, proof of concept for prediction of carcinogenicity, a chronic endpoint, with short term expression profiles in rat studies has been reported (Nie et al., 2006; Fielden et al., 2007; Thomas et al., 2007; Ellinger-Ziegelbauer et al., 2008).

Implications of the deregulation of hypertrophy associated genes

Gene expression changes indicating detoxification responses, suggested to be associated with hypertrophy, were clearly seen in the liver Tx data. However, since genes selected for a certain pathology represented a number of pathways likely due to the "poly-pathology" of the samples, selections of hypertrophy-associated genes were identified from samples showing liver hypertrophy only (Boitier et al., 2011). The expression profiles of these genes, representing a XME phenotype characterized by mainly ER proliferation, and an XME + PP phenotype, which included peroxisome proliferation, were then used to analyze the samples showing hepatobiliary toxicity as the major pathology. Hypertrophy associated genes were induced before the appearance of histological hypertrophy. Analysis for the BDN studies 4BA and 5ME revealed an XME phenotype, including upregulation of biotransformation enzyme genes. For 14SC, the upregulation of Phase I genes was not as consistent, but was still more similar to 4BA and 5ME than 7SE, at least suggesting an XME phenotype. In addition, 5ME showed a PP phenotype characterized by induction of fatty acid catabolism genes. 7SE showed neither phenotype suggesting that the observed hypertrophy was neither due to ER nor peroxisome proliferation. In a previous longer term study with this compound mitochondrial proliferation and swelling had been observed (personal communication). Thus, it appears that 7SE may present a further hypertrophy phenotype in addition to the well known ER and PP phenotypes, i.e., mitochondrial proliferation. Overall, we observed that for the adaptive hypertrophy changes, gene expression responses potentially indicating hypertrophy, could be measured before histological appearance of hypertrophy.

Bile acids as potential biomarkers of cholestasis

While statistical analysis of data obtained by global LC-MS metabonomics profiling revealed large numbers of significantly altered peaks in each study (data not shown), discrimination between toxicologically relevant metabolic changes and drug metabolites, fragments and adducts was hampered by the high complexity of the data versus the limited content of available public data bases. In addition, retention time shifts between the different laboratories performing LC-MS metabonomics analysis prevented us from performing a cross-study analysis, as conducted with Tx data. However, based on the link between bile acids and hepatobiliary function and the hypothesis that individual bile acids may serve as sensitive indicators of hepatic injury (Bai et al., 1992), a targeted bile acid analysis based on LC-MS metabonomics data was performed to determine a range of conjugated and unconjugated bile acids in urine and serum of rats treated with 4BA and 5ME, i.e. compounds inducing both hepatocellular and biliary epithelial cell injury, and 14SC, i.e. a drug inducing cholestasis in the absence of injury to the bile duct epithelium. After 14SC treatment, mainly unconjugated bile acids were increased in urine, whereas after 4BA treatment, mostly conjugated bile acids, especially taurine conjugated bile acids, were substantially elevated in both serum and urine (Table 4). In response to 5ME, an initial increase in unconjugated cholic acid was followed by a massive rise in conjugated bile acids by the end of the study.

These data may provide important information regarding the pathogenesis of liver damage induced by these compounds. In the case of 14SC, drug-induced damage to hepatocytes may have interfered with bile acid metabolism and/or conjugation, leading to accumulation of toxic unconjugated bile acids in hepatocytes, and subsequent leakage into serum and urine. This is supported by gene expression deregulations encoding enzymes involved in these processes, including evidence for decreased Coenzyme A ligation, a requirement for bile acid conjugation, and for increased thioesterase activity (data not shown). In contrast, the biliary toxicity of 4BA may

Table 4
Summary of changes in the concentration of bile acid in serum and urine in response to treatment with 4BA, 14SC and 5ME.

	Serum			Urine			Increase may indicate
	4BA	14SC	5ME	4BA	14SC	5ME	
Bile acids unconjugated	–	(↑)	–	↑	↑↑	↑↑↑	primarily hepatocyte damage
Bile acids conjugated	↑↑	(↑)	–	↑↑↑	↑	↑↑↑↑	primarily bile duct damage

have been a secondary effect arising from impaired transport of conjugated (less toxic) bile acids across the canalicular membrane of hepatocytes or leakage as a result of bile duct damage and therefore, altered biliary composition and exposure of the biliary epithelium to more concentrated bile. This suggests that increased unconjugated bile acids in urine (and serum) may be potential markers for hepatocyte damage, whereas increased conjugated bile acids in urine and serum may serve as indicators of potential biliary epithelial damage as a consequence of impaired hepatobiliary transport or direct bile duct damage. In the case of 5ME, minor hepatocellular changes preceded mixed hepatocyte and biliary epithelial cell damage and this sequence appears to be reflected by the time-related shift from a predominant rise in unconjugated bile acids to a marked increase in both conjugated and unconjugated bile acids (Table 4).

With respect to the time course, it is important to point out that—with the exception of 5ME—the increases in bile acids did not precede changes in traditional clinical chemistry hepatotoxicity markers. After 14SC treatment, the maximum increase of cholic acid in urine was measured 2 days later than the maximum increase in serum liver enzymes. In the case of 4BA, a rise in conjugated bile acids in serum was not evident at earlier time-points as compared to total bilirubin, and was even delayed in urine. On the other hand, the fold increase observed for bile acids (100×–1000× in serum and 1000×–10,000× in urine) was much higher than for total bilirubin in serum (ca. 35× in the 4BA study), suggesting that determination of conjugated vs. unconjugated bile acids, as compared to total bilirubin, may be a much more responsive parameter to diagnose hepatobiliary toxicity. In addition, the distinction between conjugated and unconjugated bile acids may allow the localization of necrotic or at least substantial cell injury to either hepatocytes or bile duct epithelial cells as evidenced by histopathology and immunolocalization of markers of proliferation and inflammation. While measurement of conjugated vs. unconjugated bilirubin in serum is possible, increases in unconjugated bilirubin may also be due to hemolysis and thus not associated with hepatotoxicity (Ozer et al., 2008).

Summary and conclusions

A synopsis of the conventional and "omics" data and their contributions to characterization of the overall sequences of events in response to treatment with compounds inducing hepatobiliary toxicity is shown in Fig. 6. Histopathologically, 4BA showed bile duct epithelial damage prior to hepatocyte necrosis, whereas 14SC was associated with early hepatocyte injury without damage to the bile duct epithelium. 5ME and 7SE showed both bile duct and hepatocyte effects without obviously distinct time courses. Analysis of the gene expression deregulations greatly enhanced the understanding of the classical observations by adding resolution at the molecular level. Common gene expression changes in liver derived from Tx data allowed us to develop a potential damage sequence on a mechanistic level in accordance with histopathological observations. Immunolocalization studies with key markers of proliferation, inflammation and tissue reorganization added molecular detail to the sites of damage observed histologically.

Targeted bile acid analysis using Mx LC-MS revealed increased conjugated bile acids in serum and urine as potential biomarkers for bile duct damage, and increased unconjugated bile acids in urine as putative indicators of intrahepatic cholestasis. These data suggest that incorporation of urine and/or serum bile acid analysis may enhance conventional safety assessment studies not only by allowing non-invasive monitoring of drug-induced liver injury during the course of a study but also by providing information with regard to the type of injury. This is particularly important in the clinical setting, where monitoring for adverse drug reactions heavily depends on reliable, mechanistically linked diagnostic and prognostic surrogate markers for target organ damage. However, further studies in preclinical

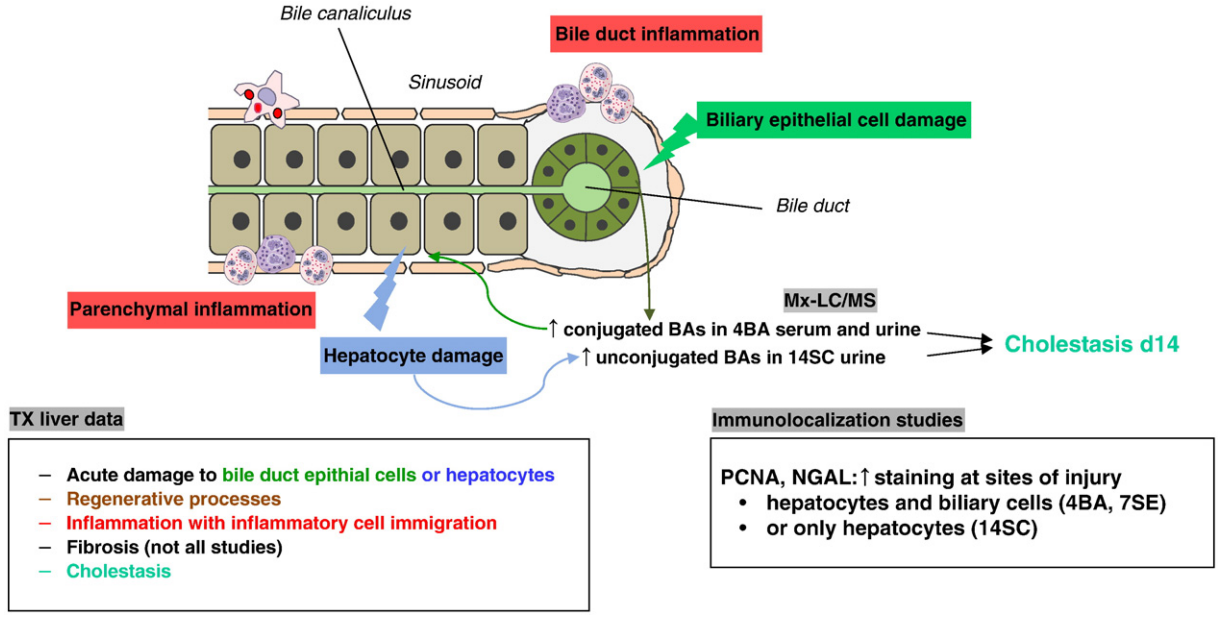

Fig. 6. Summary of histopathological changes and molecular details identified with the Tx and Mx data sets. Italics and gray background indicate histopathological observations and data types, respectively.

animal models and patients will be needed to support our findings and address translation into the clinic.

A key element of the PredTox project as compared to similar studies was the integrated omics analysis of real-life 'failed' drug candidates from participating companies. While the overall project approach was therefore not specifically tailored to develop prediction models with well-defined model toxicants, our cholestasis classification model based on a rather limited set of data shows promise. Such gene signatures may be useful in future preclinical safety assessment to identify a cholestatic potential of drug candidates, even when phenotypic manifestation of drug-induced liver injury toxicity may not have fully occurred. It remains to be established whether such signatures may also be applicable to in vitro testing as a rapid, inexpensive tool to screen and rank drug candidates early in the drug discovery process.

Supplementary material related to this article can be found online at doi:10.1016/j.taap.2010.09.022.

Acknowledgments

The contribution of all members of the PredTox Consortium (http://www.innomed-predtox.com) is gratefully acknowledged. We wish to thank all colleagues who have contributed to performance of the various studies, measurements and analyses for this project, since without their commitment, the performance of the studies and the data collection would not have been possible. We also wish to thank Eric Boitier and Katja Matheis for helpful discussions, Prof. David Tweats for his thoughtful input and guidance, and Prof Friedlieb Pfannkuch for his charismatic and efficient leadership as Project Coordinator.

The PredTox Project was supported by partial funding by the 6th Research Framework Program of the European Union (Innomed PredTox, LSHB-CT-2005-518170) and by consortium members (Bayer-Schering Pharma—formerly Bayer and Schering, Bio-Rad—formerly Ciphergen, Boehringer Ingelheim, F. Hoffmann-La Roche, Genedata, Johnson & Johnson, Lilly, Merck-Serono—formerly Merck Darmstadt and Serono, Novartis, Novo-Nordisk, Nycomed—formerly Altana, Sanofi-Aventis (D), Sanofi-Aventis (F), Schering-Plough—formerly Organon, Servier, University College Dublin, University of Hacettepe, University of Wuerzburg). We would also like to thank the scientific advisors for their support throughout the project (Timothy Gant, Christopher Gerner, John Haseldon, Peter Kasper).

References

Adler, M., Hoffmann, D., Ellinger-Ziegelbauer, H., Hewitt, P., Matheis, K., Mulrane, L., Gallagher, W.M., Callanan, J.J., Suter, L., Fountoulakis, M.M., Dekant, W., Mally, A., 2010. Assessment of candidate biomarkers of drug-induced hepatobiliary injury in preclinical toxicity studies. Toxicol. Lett. 196, 1–11.

Aslan, J.E., Thomas, G., 2009. Death by committee: organellar trafficking and communication in apoptosis. Traffic 10, 1390–1404.

Bai, C., Canfield, P.J., Stacey, N.H., 1992. Individual serum bile acids as early indicators of carbon tetrachloride- and chloroform-induced liver injury. Toxicology 75, 221–234.

Bauer, M., Bauer, I., 2002. Heme oxygenase-1: redox regulation and role in the hepatic response to oxidative stress. Antioxid. Redox Signal. 4, 749–758.

Blomme, E.A., Yang, Y., Waring, J.F., 2009. Use of toxicogenomics to understand mechanisms of drug-induced hepatotoxicity during drug discovery and development. Toxicol. Lett. 186, 22–31.

Boitier, E., Amberg, A., Barbie, V., Blichenberg, A., Brandenburg, A., Gmuender, H., Gruhler, M., McCarthy, D., Meyer, K., Riefke, B., Raschke, M., Schoonen, W., Sieber, M., Suter, L., Thomas, C.E., Sajot, N., 2011. A comparative integrated transcript analysis and functional characterization of differential mechanisms for induction of liver hypertrophy in the rat. Toxicol. Appl. Pharmacol. 252, 85–96.

Cattley, R.C., Popp, J.A., 2001. Liver. In: Haschek, W.M., Rousseaux, C.G., Wallig, M.A. (Eds.), Organ-Specific Toxicologic Pathology. Academic Press, San Diego, pp. 187–225.

Cristianini, N., Shawe-Taylor, J., 2000. An Introduction to Support Vector Machines and Other Kernel-Based Learning Methods. Cambridge University Press.

Ellinger-Ziegelbauer, H., Gmuender, H., Bandenburg, A., Ahr, H.J., 2008. Prediction of a carcinogenic potential of rat hepatocarcinogens using toxicogenomics analysis of short-term in vivo studies. Mutat. Res. 637, 23–39.

Fausto, N., Campbell, J.S., 2003. The role of hepatocytes and oval cells in liver regeneration and repopulation. Mech. Dev. 120, 117–130.

Fielden, M.R., Brennan, R., Gollub, J., 2007. A gene expression biomarker provides early prediction and mechanistic assessment of hepatic tumor induction by nongenotoxic chemicals. Toxicol. Sci. 99, 90–100.

Fon Tacer, K., Kuzman, D., Seliskar, M., Pompon, D., Rozman, D., 2007. TNF-alpha interferes with lipid homeostasis and activates acute and proatherogenic processes. Physiol. Genomics 31, 216–227.

Ganter, B., Snyder, R.D., Halbert, D.N., Lee, M.D., 2006. Toxicogenomics in drug discovery and development: mechanistic analysis of compound/class-dependent effects using the DrugMatrix database. Pharmacogenomics 7, 1025–1044.

Geier, A., Dietrich, C.G., Gerloff, T., Haendly, J., Kullak-Ublick, G.A., Stieger, B., Meier, P.J., Matern, S., Gartung, C., 2003. Regulation of basolateral organic anion transporters in ethinylestradiol-induced cholestasis in the rat. Biochim. Biophys. Acta 1609, 87–94.

Harper, J.V., Brooks, G., 2005. The mammalian cell cycle: an overview. Meth. Mol. Biol. 296, 113–153.

Hoffmann, D., Adler, M., Vaidya, V., Rached, E., Mulrane, L., Gallagher, W.M., Callanan, J.J., Gautier, J.C., Matheis, K., Staedtler, F., Dieterle, F., Brandenburg, A., Sposny, A., Hewitt, P., Ellinger-Ziegelbauer, H., Bonventre, J.V., Dekant, W., Mally, A., 2010. Performance of novel kidney biomarkers in preclinical toxicity studies. Toxicol. Sci. 116, 8–22.

Jeong, D.W., Kim, E.H., Kim, T.S., Chung, Y.W., Kim, H., Kim, I.Y., 2004. Different distributions of selenoprotein W and thioredoxin during postnatal brain development and embryogenesis. Mol. Cells 17, 156–159.

Kamisako, T., Ogawa, H., 2005. Alteration of the expression of adenosine triphosphate-binding cassette transporters associated with bile acid and cholesterol transport in the rat liver and intestine during cholestasis. J. Gastroenterol. Hepatol. 20, 1429–1434.

Kon, J., Ooe, H., Oshima, H., Kikkawa, Y., Mitaka, T., 2006. Expression of CD44 in rat hepatic progenitor cells. J. Hepatol. 45, 90–98.

Loflin, J., Lopez, N., Whanger, P.D., Kioussi, C., 2006. Selenoprotein W during development and oxidative stress. J. Inorg. Biochem. 100, 1679–1684.

Malhi, H., Gores, G.J., Lemasters, J.J., 2006. Apoptosis and necrosis in the liver: a tale of two deaths? Hepatology 43, S31–S44.

Man, M.Z., Dyson, G., Johnson, K., Liao, B., 2004. Evaluating methods for classifying expression data. J. Biopharm. Stat. 14, 1065–1084.

Mattes, W.B., Pettit, S.D., Sansone, S.A., Bushel, P.R., Waters, M.D., 2004. Database development in toxicogenomics: issues and efforts. Environ. Health Perspect. 112, 495–505.

Mazzocca, A., Carloni, V., Sciammetta, S., Cordella, C., Pantaleo, P., Caldini, A., Gentilini, P., Pinzani, M., 2002. Expression of transmembrane 4 superfamily (TM4SF) proteins and their role in hepatic stellate cell motility and wound healing migration. J. Hepatol. 37, 322–330.

Minter, R.M., Fan, M.H., Sun, J., Niederbichler, A., Ipaktchi, K., Arbabi, S., Hemmila, M.R., Remick, D.G., Wang, S.C., Su, G.L., 2005. Altered Kupffer cell function in biliary obstruction. Surgery 138, 236–245.

Mulrane, L., Rexhepaj, E., Smart, V., Callanan, J.J., Orhan, D., Eldem, T., Mally, A., Schroeder, S., Meyer, K., Wendt, M., O'Shea, D., Gallagher, W.M., 2008. Creation of a digital slide and tissue microarray resource from a multi-institutional predictive toxicology study in the rat: an initial report from the PredTox group. Exp. Toxicol. Pathol. 60, 235–245.

Murphy, F.R., Issa, R., Zhou, X., Ratnarajah, S., Nagase, H., Arthur, M.J., Benyon, C., Iredale, J.P., 2002. Inhibition of apoptosis of activated hepatic stellate cells by tissue inhibitor of metalloproteinase-1 is mediated via effects on matrix metalloproteinase inhibition: implications for reversibility of liver fibrosis. J. Biol. Chem. 277, 11069–11076.

Nakamura, H., Hirata, K., Yamashiro, K., Hiranuma, K., Shibata, K., Higashi, K., Morita, T., Hirano, H., 1994. Increase of hepatic mRNAS of profilin, actin and extracellular matrix proteins after carbon tetrachloride treatment and partial hepatectomy in rats. Biochem. Biophys. Res. Commun. 198, 568–573.

Nie, A.Y., McMillian, M., Brandon Parker, J., Leone, A., Bryant, S., Yieh, L., Bittner, A., Nelson, J., Carmen, A., Wan, J., Lord, P.G., 2006. Predictive toxicogenomics approaches reveal underlying molecular mechanisms of nongenotoxic carcinogenicity. Mol. Carcinog. 45, 914–933.

Ozer, J., Ratner, M., Shaw, M., Bailey, W., Schomaker, S., 2008. The current state of serum biomarkers of hepatotoxicity. Toxicology 245, 194–205.

Raghavan, N., Amaratunga, D., Nie, A.Y., McMillian, M., 2005. Class prediction in toxicogenomics. J. Biopharm. Stat. 15, 327–341.

Ringner, M., Peterson, C., Khan, J., 2002. Analyzing array data using supervised methods. Pharmacogenomics 3, 403–415.

Rocca-Serra, P., Brandizi, M., Eamonn, M., Sklyar, N., Taylor, C., Begley, K., Field, D., Harris, S., Hide, W., Hofmann, O., Neumann, S., Sterk, P., Tong, W., Sansone, S.A., 2010. ISA software suite: supporting standards-compliant experimental annotation and enabling curation at the community level. Bioinformatics 26, 2354–2356.

Salter, A.H., Nilsson, K.C., 2003. Informatics and multivariate analysis of toxicogenomics data. Curr. Opin. Drug Discov. Dev. 6, 117–122.

Schumann, R.R., Zweigner, J., 1999. A novel acute-phase marker: lipopolysaccharide binding protein (LBP). Clin. Chem. Lab. Med. 37, 271–274.

Stupack, D.G., Cheresh, D.A., 2002. Get a ligand, get a life: integrins, signaling and cell survival. J. Cell Sci. 115, 3729–3738.

Sunil, V.R., Patel, K.J., Nilsen-Hamilton, M., Heck, D.E., Laskin, J.D., Laskin, D.L., 2007. Acute endotoxemia is associated with upregulation of lipocalin 24p3/Lcn2 in lung and liver. Exp. Mol. Pathol. 83, 177–187.

Suter, L., Schroeder, S., Meyer, K., Gautier, J.C., Amberg, A., Wendt, M., Gmuender, H., Mally, A., Boitier, E., Ellinger-Ziegelbauer, H., Mattheis, K., Pfannkuch, F., 2011. EU Framework 6 Project: Predictive Toxicology (PredTox)—overview and outcome. Toxicol. Appl. Pharmacol. 252, 73–84.

Thomas, R.S., O'Connell, T.M., Pluta, L., Wolfinger, R.D., Yang, L., Page, T.J., 2007. A comparison of transcriptomic and metabonomic technologies for identifying biomarkers predictive of two-year rodent cancer bioassays. Toxicol. Sci. 96, 40–46.

White, P., Brestelli, J.E., Kaestner, K.H., Greenbaum, L.E., 2005. Identification of transcriptional networks during liver regeneration. J. Biol. Chem. 280, 3715–3722.

Xu, H.B., Gong, Y.P., Cheng, J., Chu, Y.W., Xiong, S.D., 2005. CXCL16 participates in pathogenesis of immunological liver injury by regulating T lymphocyte infiltration in liver tissue. World J. Gastroenterol. 11, 4979–4985.

Yuan, H., Zhang, H., Wu, X., Zhang, Z., Du, D., Zhou, W., Zhou, S., Brakebusch, C., Chen, Z., 2009. Hepatocyte-specific deletion of Cdc42 results in delayed liver regeneration after partial hepatectomy in mice. Hepatology 49, 240–249.